Hadron-quark phase transition in dense matter and neutron stars

G. F. Burgio,[1] M. Baldo,[1] P. K. Sahu,[2] and H.-J. Schulze[1]
[1]*Istituto Nazionale di Fisica Nucleare, Sezione di Catania, Corso Italia 57, I-95129 Catania, Italy*
[2]*Institute of Physics, Sachivalaya Marg, Bubhaneswar-751 005, India*
(Received 3 June 2002; published 26 August 2002)

We study the hadron-quark phase transition in the interior of neutron stars (NS's). We calculate the equation of state (EOS) of hadronic matter using the Brueckner-Bethe-Goldstone formalism with realistic two-body and three-body forces, as well as a relativistic mean field model. For quark matter we employ the MIT bag model constraining the bag constant by using the indications coming from the recent experimental results obtained at the CERN SPS on the formation of a quark-gluon plasma. We find it necessary to introduce a density-dependent bag parameter and the corresponding consistent thermodynamical formalism. We calculate the structure of NS interiors with the EOS comprising both phases, and we find that the NS maximum masses fall in a relatively narrow interval, $1.4\,M_{\odot} \leqslant M_{\max} \leqslant 1.7 M_{\odot}$. The precise value of the maximum mass turns out to be only weakly correlated with the value of the energy density at the assumed transition point in nearly symmetric nuclear matter.

DOI: 10.1103/PhysRevC.66.025802 PACS number(s): 26.60.+c, 21.65.+f, 24.10.Cn, 97.60.Jd

I. INTRODUCTION

The properties of nuclear matter at high density play a crucial role for building models of neutron stars NS's [1]. The observed NS masses are in the range of $\approx(1-2)M_{\odot}$ (where $M_{\odot}$ is the mass of the sun, $M_{\odot}=1.99\times10^{33}$ g), and the radii are of the order of 10 km. The characteristics of the core of the NS's influence most strongly the value of the maximum mass. The matter inside this core possesses densities ranging from a few times ρ_0 (≈ 0.17 fm^{-3}, the normal nuclear matter density) to one order of magnitude higher. Moreover, the equation of state (EOS) at such high densities is the main ingredient for determining the structure parameters of NS's, such as mass and radius. Therefore, a detailed knowledge of the EOS is required for densities $\rho \gg \rho_0$, where a description of matter only in terms of nucleons and leptons may be inadequate. In fact, at densities $\rho \gg \rho_0$ several species of other particles, such as hyperons and Δ isobars, may appear, and meson condensations may take place; also, ultimately, at very high densities, nuclear matter is expected to undergo a phase transition to a quark-gluon plasma [2]. The specific goal of the theory is to study the nature of this plasma and understand the phase transitions between different states. However, the exact value of the transition density to quark matter is unknown and still a matter of recent debate not only in astrophysics, but also within the theory of high-energy heavy-ion collisions.

In this paper, we propose a method to determine a range of values of the maximum mass of NS's taking into account the phase transition from hadronic matter to quark matter inside the neutron star. The transition point is constrained from recent heavy-ion collision data. Therefore to perform such calculations, we describe the hadron phase of matter by using two different equations of state, i.e., a microscopic nonrelativistic EOS obtained in the Brueckner-Bethe-Goldstone (BBG) theory [3], and a more phenomenological relativistic mean field model [4]. The deconfined quark matter phase is treated by adopting the popular MIT bag model [5]. In a previous paper [6] the bag ''constant,'' B, which is a parameter of the bag model, was constrained to be compatible with the recent experimental results obtained at CERN on the formation of a quark-gluon plasma [7], recently confirmed by RHIC preliminary results [8].

However, it is not obvious if the information on the nuclear EOS from high-energy heavy-ion collisions can be related to the physics of neutron star interiors. The possible quark-gluon plasma produced in heavy-ion collisions is expected to be characterized by small baryon density and high temperature, while the possible quark phase in neutron stars appears at high baryon density and low temperature. If one adopts for the hadronic phase a noninteracting gas model of nucleons, antinucleons, and pions, the original MIT bag model predicts that the deconfined phase occurs at an almost constant value of the quark-gluon energy density, irrespective of the thermodynamical conditions of the system [9]. For this reason, it is popular to draw the transition line between the hadronic and the quark phase at a constant value of the energy density, which was estimated to fall in the interval between 0.5 and 2 GeV fm^{-3} [10]. This is consistent with the value of about 1 GeV fm^{-3} reported by CERN experiments. The close relation between the physics of neutron stars and of heavy-ion collisions is also emphasized by a recent conjecture that there could be three phases in heavy-ion collisions at SPS and RHIC energies, equivalent to the pure quark phase, mixed phase, and pure hadron phase appearing in neutron stars. These three phases correspond to (a) an explosive hard quark-gluon phase, (b) a mixed soft phase (a sort of plateau), and (c) a hadronic phase. Considering these three phases in a heavy-ion collision model, the first available RHIC data could be well described [11].

The value of 1 GeV fm^{-3} must be considered only an indicative estimate of the transition energy density at zero or nearly zero temperature, as needed in neutron star studies, and it appears mandatory to explore the sensitivity of the results on the precise value of the assumed transition energy density. In this work we present systematic calculations of neutron star structure, where the hadronic EOS, which can be considered well established, is implemented with the pos-

sible transition to the deconfined phase described by different parametrizations of the MIT bag model. The transition energy density in nearly symmetric nuclear matter at zero temperature is allowed to vary within a range of values which can be considered still compatible with the CERN and RHIC data. The calculations will indicate the sensitivity of the results on the assumed transition point and the possible correlation between neutron star properties and the transition energy density value. In particular, we will see that the maximum neutron star mass is only weakly correlated with the transition energy density value.

This paper is organized as follows. In Sec. II we discuss the EOS for the hadronic phase of a neutron star, i.e., the BBG and the relativistic mean field models. In Sec. III we apply the MIT bag model to the description of the quark phase of the neutron star. In Sec. IV we present our results and finally in Sec. V we draw some conclusions.

II. HADRONIC PHASE

A. Brueckner-Hartree-Fock theory

The BBG theory is based on a linked cluster expansion of the energy per nucleon of nuclear matter (see Ref. [3], Chap. 1 and references therein). The basic ingredient in this many-body approach is the Brueckner reaction matrix G, which is the solution of the Bethe-Goldstone equation

$$G[n;\omega]=v+\sum_{k_a k_b} v\,\frac{|k_a k_b\rangle Q\langle k_a k_b|}{\omega-e(k_a)-e(k_b)}\,G[n;\omega], \qquad (1)$$

where v is the bare nucleon-nucleon (NN) interaction, n is the nucleon number density, and ω the starting energy. The single-particle energy $e(k)$ (assuming $\hbar=1$ here and throughout the paper)

$$e(k)=e(k;n)=\frac{k^2}{2m}+U(k;n) \qquad (2)$$

and the Pauli operator Q determine the propagation of intermediate baryon pairs. The Brueckner-Hartree-Fock (BHF) approximation for the single-particle potential $U(k;n)$ using the *continuous choice* is

$$U(k;n)=\mathrm{Re}\sum_{k'\le k_F}\langle kk'|G[n;e(k)+e(k')]|kk'\rangle_a, \qquad (3)$$

where the subscript a indicates antisymmetrization of the matrix element. Due to the occurrence of $U(k)$ in Eq. (2), they constitute a coupled system that has to be solved in a self-consistent manner for several Fermi momenta of the particles involved. In the BHF approximation the energy per nucleon is

$$\frac{E}{A}=\frac{3}{5}\frac{k_F^2}{2m}+\frac{1}{2n}\sum_{k,k'\le k_F}\langle kk'|G[n;e(k)+e(k')]|kk'\rangle_a. \qquad (4)$$

In this scheme, the only input quantity we need is the bare NN interaction v in the Bethe-Goldstone equation (1). In this sense the BBG approach can be considered as a microscopic one. The nuclear EOS can be calculated with good accuracy in the Brueckner two-hole-line approximation with the continuous choice for the single-particle potential, since the results in this scheme are quite close to the calculations, which include also the three-hole-line contribution [12]. In the calculations reported here, we have used the Paris potential [13] as the two-nucleon interaction.

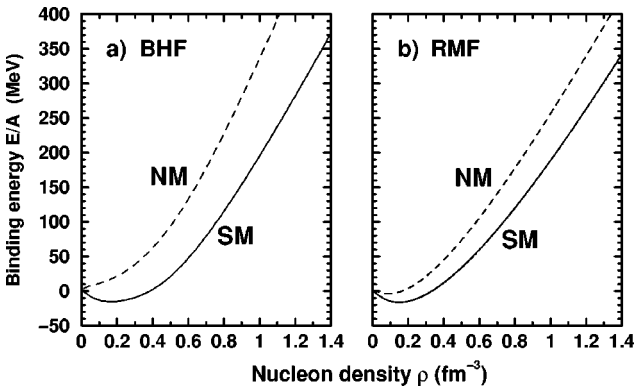

FIG. 1. The BHF [RMF] equation of state is displayed in panel (a) [panel (b)] for symmetric matter (solid line) and pure neutron matter (dashed line).

However, it is commonly known that nonrelativistic calculations, based on purely two-body interactions, fail to reproduce the correct saturation point of symmetric nuclear matter, and three-body forces (TBF's) among nucleons are needed to correct this deficiency. In this work the so-called Urbana model will be used, which consists of an attractive term due to the two-pion exchange with excitation of an intermediate Δ resonance, and a repulsive phenomenological central term [14]. We introduced the same Urbana three-nucleon model within the BHF approach (for more details see Ref. [15]). In our approach the TBF is reduced to a density-dependent two-body force by averaging over the position of the third particle, assuming that the probability of having two particles at a given distance is reduced according to the two-body correlation function. The corresponding nuclear matter EOS fulfills several requirements, namely, (i) it reproduces the correct nuclear matter saturation point, (ii) the incompressibility is compatible with the values extracted from phenomenology, (iii) the symmetry energy is compatible with nuclear phenomenology, and (iv) the causality condition is always fulfilled. The equation of state is displayed in Fig. 1(a), for symmetric matter (solid line) and pure neutron matter (dashed line).

Recently, we have included the hyperon degrees of freedom within the same approximation to calculate the nuclear EOS needed to describe the NS interior [16]. We have included the Σ^- and Λ hyperons. To this purpose, one needs also nucleon-hyperon (NY) and hyperon-hyperon (YY) interactions [16,17]. However, because of a lack of experimental data, the hyperon-hyperon interaction has been neglected in the first approximation in this work, whereas for the NY interaction the Nijmegen soft-core model [18] has been adopted.

Once hyperons and leptons are introduced, the total EOS

can be calculated for a given composition of the baryon components. This allows the determination of the chemical potentials of all species which are the fundamental input for the equations of chemical equilibrium:

$$\mu_n = \mu_p + \mu_e , \tag{5}$$

$$\mu_e = \mu_\mu , \tag{6}$$

$$2\mu_n = \mu_p + \mu_\Sigma , \tag{7}$$

$$\mu_n = \mu_\Lambda . \tag{8}$$

Since we are looking at neutron stars after neutrinos have escaped, we set the neutrino chemical potentials equal to zero. The above equations must be supplemented with two other conditions, i.e., charge neutrality and baryon number conservation. These are

$$\rho_p = \rho_e + \rho_\mu + \rho_\Sigma , \tag{9}$$

$$\rho = \rho_n + \rho_p + \rho_\Sigma + \rho_\Lambda . \tag{10}$$

The last two conditions allow the unique solution of a closed system of equations, yielding the equilibrium fractions of the baryon and lepton species for each fixed baryon density. The latter determine the actual detailed composition of the dense matter and therefore the EOS to be used in the interior of neutron stars. Finally, from the knowledge of the equilibrium composition one determines the equation of state, i.e., the relation between pressure P and energy density ϵ as a function of baryon density ρ. It can be easily obtained from the thermodynamical relation

$$P = -\frac{dE}{dV}, \tag{11}$$

with E the total energy and V the total volume. Equation (11) can be explicitly worked out in terms of the baryonic and leptonic energy densities ϵ_B and ϵ_L,

$$P = -\frac{dE}{dV} = P_B + P_L , \tag{12}$$

$$P_B = \rho^2 \frac{d(\epsilon_B/\rho)}{d\rho}, \quad P_L = \rho^2 \frac{d(\epsilon_L/\rho)}{d\rho}. \tag{13}$$

The total baryonic energy density ϵ_B is obtained by adding the energy densities of each species ϵ_i, which in turn are calculated by taking into account the interaction of the species i with the surrounding medium (see Ref. [16] and references therein),

$$\epsilon_B = \epsilon_N + \epsilon_\Sigma + \epsilon_\Lambda . \tag{14}$$

As far as the leptons are concerned, at those high densities electrons are a free ultrarelativistic gas, whereas muons are relativistic. Therefore their energy densities ϵ_L and pressures P_L are well known from textbooks; see, e.g., Ref. [1].

B. Relativistic mean field model

In the present work, we have also considered a hadronic EOS based on the framework of a relativistic approach, where one usually starts from a local, renormalizable field theory with baryons and explicit meson degrees of freedom. The theory is chosen to be renormalizable in order to fix the coupling constants and the mass parameters by empirical properties of nuclear matter at saturation. As a starting point, one chooses the mean field approximation, which should be reasonably good at very high densities (a few times nuclear matter density).

In 1974, Walecka first proposed the mean field model [4,19], where the coupling constants were chosen in such a way that it fitted nuclear matter binding energy and saturation density. However, in this model the value of the nuclear matter incompressibility at saturation is quite high. In order to reproduce the correct value, an extension of the Walecka model was done later, called the nonlinear Walecka model [20–23]. This model has been proven quite successful in describing the properties of nuclei [4] over a wide range of the periodic table. Thus it is reasonable to use such a model to describe the hadronic phase in a region where the nuclear densities are not too large in comparison with the nuclear matter density.

The equation of state for hadrons is calculated in the framework of mean field theory using the nonlinear Walecka Lagrangian [20,21,23]

$$\begin{aligned}
\mathcal{L}(x) &= \sum_i \bar{\psi}_i (i\gamma^\mu \partial_\mu - m_i + g_{\sigma i}\sigma + g_{\omega i}\omega_\mu \gamma^\mu - g_{\rho i}\rho_\mu^a \gamma^\mu T_a)\psi_i \\
&\quad - \frac{1}{4}\omega^{\mu\nu}\omega_{\mu\nu} + \frac{1}{2}m_\omega^2 \omega_\mu \omega^\mu \\
&\quad + \frac{1}{2}(\partial_\mu \sigma \partial^\mu \sigma - m_\sigma^2 \sigma^2) - \frac{1}{4}\rho_{\mu\nu}^a \rho_a^{\mu\nu} + \frac{1}{2}m_\rho^2 \rho_\mu^a \rho_a^\mu \\
&\quad - \frac{1}{3}b m_N (g_{\sigma N}\sigma)^3 - \frac{1}{4}c(g_{\sigma N}\sigma)^4 \\
&\quad + \sum_l \bar{\psi}_l (i\gamma^\mu \partial_\mu - m_l)\psi_l .
\end{aligned} \tag{15}$$

This Lagrangian includes nucleons, Λ and Σ^- hyperons (denoted by a subscript i), leptons (denoted by l), and σ, ω, and ρ mesons. The meson fields interact with baryons through linear couplings and the coupling constants are different for nonstrange and strange baryons. The ω and ρ masses are chosen to be their physical masses. The equation of state is obtained through the mean field ansatz. In this case one can define effective masses ($\overline{m}_i$) and chemical potentials ($\overline{\mu}_i$) for the baryons as

$$\begin{aligned}
\overline{m}_i &= m_i - g_{\sigma i}\overline{\sigma}, \\
\overline{\mu}_i &= \mu_i - g_{\omega i}\overline{\omega}_0 - T_3 g_{\rho i}\overline{\rho}_0^3,
\end{aligned} \tag{16}$$

where $\overline{\omega}_0$, $\overline{\sigma}$, and $\overline{\rho}_0^3$ are the nonzero vacuum expectation values of the meson fields. T_3 is the value of the z compo-

nent of the isospin of baryon i, whereas μ_i is the bare chemical potential. In neutron star matter the chemical potentials must fulfill the conditions of equilibrium under weak interaction, i.e.,

$$\overline{\mu}_n = \overline{\mu}_p + \mu_e, \quad \mu_e = \mu_\mu, \tag{17}$$

$$2\overline{\mu}_n = \overline{\mu}_p + \overline{\mu}_\Sigma, \quad \overline{\mu}_n = \overline{\mu}_\Lambda. \tag{18}$$

Moreover, the condition of charge neutrality (9) must be satisfied as well as the baryon number conservation (10). By minimizing the energy at fixed baryon density, one gets the mean field values of $\overline{\omega}_0$, $\overline{\sigma}$, and $\overline{\rho}_0^3$. Then the expressions of the energy density and pressure are readily obtained as

$$\epsilon = \frac{1}{2}m_\omega^2\overline{\omega}_0^2 + \frac{1}{2}m_\rho^2(\overline{\rho}_0^3)^2 + \frac{1}{2}m_\sigma^2\overline{\sigma}^2 + \frac{1}{3}bm_N(g_{\sigma N}\overline{\sigma})^3 + \frac{1}{4}c(g_{\sigma N}\overline{\sigma})^4 + \sum_i \epsilon_{\mathrm{FG}}(\overline{m}_i, \overline{\mu}_i) + \sum_l \epsilon_{\mathrm{FG}}(m_l, \mu_l), \tag{19}$$

$$P = \frac{1}{2}m_\omega^2\overline{\omega}_0^2 + \frac{1}{2}m_\rho^2(\overline{\rho}_0^3)^2 - \frac{1}{2}m_\sigma^2\overline{\sigma}^2 - \frac{1}{3}bm_N(g_{\sigma N}\overline{\sigma})^3 - \frac{1}{4}c(g_{\sigma N}\overline{\sigma})^4 + \sum_i P_{\mathrm{FG}}(\overline{m}_i, \overline{\mu}_i) + \sum_l P_{\mathrm{FG}}(m_l, \mu_l), \tag{20}$$

where ϵ_{FG} and P_{FG} represent the noninteracting fermion contributions to the energy density and the pressure. The nonlinear Walecka model has eight parameters out of which five are determined by the properties of nuclear matter. These are the nucleon couplings to scalar (g_σ/m_σ), isovector (g_ρ/m_ρ), and vector mesons (g_ω/m_ω) and the two coefficients b and c. These are obtained by fitting saturation values of nuclear matter, i.e., binding energy per nucleon (~ -16 MeV), baryon density (~ 0.15 fm^{-3}), and Landau mass ($0.83m_N$). The symmetry energy coefficient and the compressibility are taken equal to, respectively, 30 and 260 MeV, the same as in BHF calculations and close to estimated values from monopole oscillations in nuclei [24].

The other three coupling constant parameters of the hyperon couplings (ratio of hyperon-meson and nucleon-meson couplings) are not well known. Since hyperons are not present in nuclear matter, these cannot be determined from the nuclear matter properties. Moreover, from the analysis of experimental data on hypernuclei, one cannot fix these parameters in a unique way. Therefore, we fix these parameters by assuming the potentials experienced by Σ^- hyperons to be the same as that of Λ, e.g., -30 MeV in the present calculations. First, we choose the value of hyperon couplings for scalar mesons as 2/3 (similar to the quark counting value for Λ and Σ^-). Next, using the above assumption for the hyperon potentials, the values of the hyperon couplings for vector mesons are calculated and the hyperon couplings for isovector mesons are set equal to those for vector mesons assuming vector dominance. For further details, the reader is referred to Refs. [25,26] and references therein. The resulting equation of state is displayed in Fig. 1(b), for symmetric matter (solid line) and pure neutron matter (dashed line).

III. QUARK PHASE

We now turn to the description of the bulk properties of uniform quark matter, deconfined from the β-stable hadronic matter mentioned in the preceding section, by using the MIT bag model [5]. We begin with the thermodynamic potential of q quarks, where $q = u,d,s$ denote up, down, and strange quarks, expressed as a sum of the kinetic term and the one-gluon-exchange term [2,27],

$$\Omega_q = -\frac{3m_q^4}{8\pi^2}\left[\frac{\eta_q x_q}{3}(2x_q^2 - 3) + \ln(x_q + \eta_q)\right] + \frac{3m_q^4\alpha_s}{4\pi^3} \times \left\{2[\eta_q x_q - \ln(x_q + \eta_q)]^2 - \frac{4}{3}x_q^4 + 2\ln(\eta_q) + 4\ln\left(\frac{\sigma_{\mathrm{ren}}}{m_q\eta_q}\right)[\eta_q x_q - \ln(x_q + \eta_q)]\right\}, \tag{21}$$

where m_q and μ_q are the q current quark mass and chemical potential, respectively, and $x_q = \sqrt{\mu_q^2 - m_q^2}/m_q$, $\eta_q = \sqrt{1 + x_q^2} = \mu_q/m_q$. α_s denotes the QCD fine structure constant, whereas σ_{ren} is the renormalization point, $\sigma_{\mathrm{ren}} = 313$ MeV. In this work we will consider massless u and d quarks, in which case the above expression reduces to

$$\Omega_q = -\frac{\mu_q^4}{4\pi^2}\left(1 - \frac{2\alpha_s}{\pi}\right) \quad (q = u,d). \tag{22}$$

The number density ρ_q of q quarks is related to Ω_q via

$$\rho_q = -\frac{\partial\Omega_q}{\partial\mu_q}, \tag{23}$$

and the total energy density and pressure for the quark system are given by

$$\epsilon_Q = \sum_q (\Omega_q + \mu_q\rho_q) + B, \tag{24}$$

$$P_Q = -\sum_q \Omega_q - B, \tag{25}$$

where B is the energy density difference between the perturbative vacuum and the true vacuum, i.e., the bag constant. In the original MIT bag model the bag constant has the value $B \approx 55$ MeV fm^{-3}, which is quite small when compared with the ones (≈ 210 MeV fm^{-3}) estimated from lattice calculations [28]. In this sense B can be considered as a free parameter. The composition of β-stable quark matter is determined by imposing the condition of equilibrium under weak interactions for the following processes:

$$u+e^- \rightarrow d+\nu_e, \tag{26}$$

$$u+e^- \rightarrow s+\nu_e, \tag{27}$$

$$d \rightarrow u+e^-+\overline{\nu_e}, \tag{28}$$

$$s \rightarrow u+e^-+\overline{\nu_e}, \tag{29}$$

$$s+u \rightarrow d+u. \tag{30}$$

In neutrino-free matter ($\mu_{\nu_e}=\mu_{\overline{\nu_e}}=0$), the above equations imply for the chemical potentials

$$\mu_d=\mu_s=\mu, \tag{31}$$

$$\mu=\mu_u+\mu_e. \tag{32}$$

As in baryonic matter, the relations for chemical equilibrium must be supplemented with the charge neutrality condition and the total baryon number conservation:

$$\frac{2}{3}\rho_u-\frac{1}{3}\rho_d-\frac{1}{3}\rho_s-\rho_e=0, \tag{33}$$

$$\rho=\frac{1}{3}(\rho_u+\rho_d+\rho_s). \tag{34}$$

It can easily be demonstrated that, in the case of massless *u*, *d*, and *s* quarks, the equilibrium solution reads

$$\rho_u=\rho_d=\rho_s, \quad \rho_e=0, \tag{35}$$

and consequently the equation of state is

$$P_Q=\frac{1}{3}(\epsilon_Q-4B). \tag{36}$$

Here one should notice that the above expressions hold in the case of constant *B*. If the bag constant is density dependent, all thermodynamical relations must be reformulated [29].

In this case it is convenient to consider the first two terms on the right-hand side of Eq. (24) as a function of density. The density of each flavor component q is related to the Fermi momentum $p_F^{(q)}$ in the usual way,

$$\rho_q=\frac{g}{6\pi^2}[p_F^{(q)}]^3, \tag{37}$$

where $g=6$ is the spin and color degeneracy factor. If we denote by ρ the total baryon density, the chemical potential μ_q for each flavor component q can be written

$$\mu_q=E_F^{(q)}+\frac{dB}{d\rho_q}, \tag{38}$$

where $E_F^{(q)}$ is the kinetic Fermi energy for the q component, eventually including the perturbative corrections. The second term on the right-hand side of Eq. (38) modifies the usual relationship between chemical potential and Fermi energy and is absent for a density-independent parameter *B*. This term in turn modifies the relationship between chemical potential and density in an obvious way. These additional terms are essential for the consistency of the different thermodynamical relationships. In particular, the usual expressions for the pressure

$$P_Q=\rho\frac{d\epsilon_Q}{d\rho}-\epsilon_Q=\sum_q \mu_q\rho_q-\epsilon_Q \tag{39}$$

hold true provided the additional term involving the derivative of the bag parameter is included, which is absent in Eq. (25), where the free Fermi gas expression for Ω_q is assumed. In our calculations both chemical potentials and pressure have been calculated including the additional terms, thus fulfilling the correct thermodynamical relationships. We found that this additional term, coming from the density dependence of the bag parameter, gives a substantial contribution. In particular, it reduces strongly the value of the pressure especially in the mixed phase region, as described in the next section.

IV. RESULTS AND DISCUSSION

We try to determine a range of possible values for *B* by exploiting the experimental data obtained at the CERN SPS, where several experiments using high-energy beams of Pb nuclei reported the (indirect) evidence for the formation of a quark-gluon plasma [7]. The resulting picture is the following: during the early stages of the heavy-ion collision, a very hot and dense state (fireball) is formed, whose energy materializes in the form of quarks and gluons strongly interacting with each other, exhibiting features consistent with expecta-

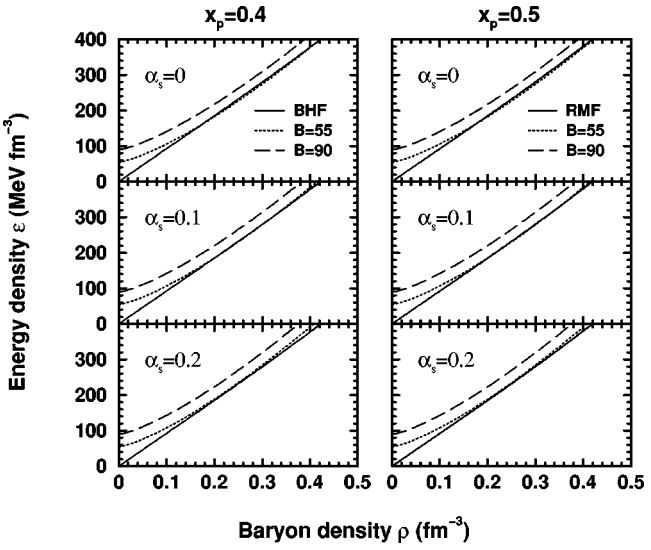

FIG. 2. The energy density is displayed vs the baryon density for almost symmetric matter. Panels on the left-hand side show BHF calculations ($x_p=0.4$, solid line), whereas panels on the right-hand side show the ones obtained with the relativistic mean field model ($x_p=0.5$, solid line). The dotted (dashed) lines represent calculations for *u*, *d* quark matter within the MIT bag model, performed with $B=55$ MeV fm^{-3} ($B=90$ MeV fm^{-3}) and several values of the QCD coupling constant α_s.

TABLE I. The values of B_∞ (in MeV fm^{-3}) are displayed vs those of the energy density (in GeV fm^{-3}) in *u*, *d* quark matter at the transition point for $\alpha_s=0$, 0.1. The corresponding values of the baryonic densities $\overline{\rho}$ (in fm^{-3}) at transition are deduced from the BHF and RMF hadronic equations of state.

EOS	ϵ_Q	$\overline{\rho}$	$B_\infty^{\alpha_s=0}$	$B_\infty^{\alpha_s=0.1}$
BHF	0.8	0.76	36.4	19.6
	1.1	0.97	51.1	27.9
	1.5	1.22	77.4	45.8
RMF	0.8	0.76	37.9	21.0
	1.1	0.98	37.8	14.3
	1.5	1.23	55.4	23.4

tions from a plasma of deconfined quarks and gluons [30]. Subsequently, the ''plasma'' cools down and becomes more dilute up to the point where, at an energy density of about 1 GeV fm^{-3} and temperature $T\approx 170$ MeV, the quarks and gluons hadronize. The expansion is fast enough so that no mixed hadron-quark equilibrium phase is expected to occur, and no weak process can play a role. According to the analysis of those experiments, the quark-hadron transition takes place at about seven times normal nuclear matter energy density ($\epsilon_0\approx 156$ MeV fm^{-3}).

In the MIT bag model, the structure of the QCD phase diagram in the chemical potential and temperature plane is determined by only one parameter, *B*, although the phase diagram for the transition from nuclear matter to quark matter is schematic and not yet completely understood, particularly in light of recent investigations on a color superconducting phase of quark matter [31]. In our analysis we assume that the transition to a quark-gluon plasma is determined by the value of the energy density alone (for a given asymmetry). With this assumption and taking the hadron to quark matter transition energy density from the CERN experiments, we estimate in the following the value of *B* and its possible density dependence.

A. Phase transition in symmetric nuclear matter

First, we calculate the EOS for cold asymmetric nuclear matter characterized by a proton fraction $x_p=0.4$ (the one for Pb nuclei accelerated at CERN-SPS energies) in the BHF formalism with two-body and three-body forces (as described earlier). We perform the same calculation in the relatistic mean field (RMF) approach using $x_p=0.5$. Then we calculate the EOS for *u* and *d* quark matter using Eq. (24). First we use a constant, density-independent, *B*. The results are shown in Fig. 2. The solid lines represent the BHF (left panel) and the RMF (right panel) calculation of the energy density. The dotted (dashed) lines represent the quark matter equation of state calculated for $B=55$ MeV fm^{-3} ($B=90$ MeV fm^{-3}), and several values of the QCD coupling constant α_s. We find that at very low baryon density the quark matter energy density is always higher than that of nuclear matter, independently of the value of *B*. Therefore nuclear matter is the favorite state. However, for $B=55$ MeV fm^{-3}, the two energy densities become equal at a certain value of nuclear density. Unfortunately this crossing takes place at normal nuclear matter density, both in the BHF and the RMF approach. Therefore we try a larger value of *B*. Since the expression of the quark matter energy density is linear in *B* [see Eq. (24)], an increase of *B* means an overall shift towards larger energy densities. The two curves can cross now at a slightly larger baryon density, but still much smaller than the desired point, i.e., $E/V\approx 7\epsilon_0\approx 1.1$ GeV fm^{-3}. No crossing at all is present above some limiting value of *B*. In Fig. 2 we show for completeness also the limiting case of $B=90$ MeV fm^{-3}, where the nuclear matter energy density is always smaller than that of quark matter. These results are not very sensitive to the value of α_s.

Therefore, we assume a density dependent *B* (an eventual dependence of *B* on the asymmetry x_p is not considered at this stage). In the literature there are attempts to understand the density dependence of *B* [32,33]; however, currently the results are highly model dependent and no definite picture has come out yet. Therefore, we attempt to provide effective parametrizations for this density dependence, trying to cover a wide range by considering some extreme choices. Our parametrizations are constructed in such a way that at asymptotic densities *B* has some finite value B_∞. In order to fix B_∞ we proceed in the following way. The energy density for *u*, *d* quark matter reads

$$\epsilon_Q(\rho,x_p)=B(\rho)+\frac{3}{4}\left[\frac{\pi^2}{(1-2\alpha_s/\pi)}\right]^{1/3}\times[(1+x_p)^{4/3}+(2-x_p)^{4/3}]\rho^{4/3}. \quad (40)$$

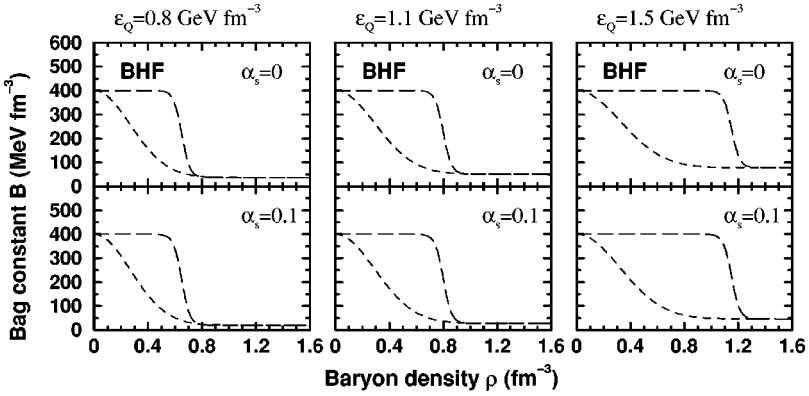

FIG. 3. The bag constant *B* is displayed vs the baryon density ρ. Two parametrizations are adopted, i.e., a Gaussian one (short dashed lines) and a Woods-Saxon–like one (long dashed lines). The left, central, and right panels correspond to different transition energy densities $\epsilon_Q=0.8$, 1.1, and 1.5 GeV fm^{-3}. Calculations are performed for the BHF nucleonic equation of state, and for two values of $\alpha_s=0$, 0.1.

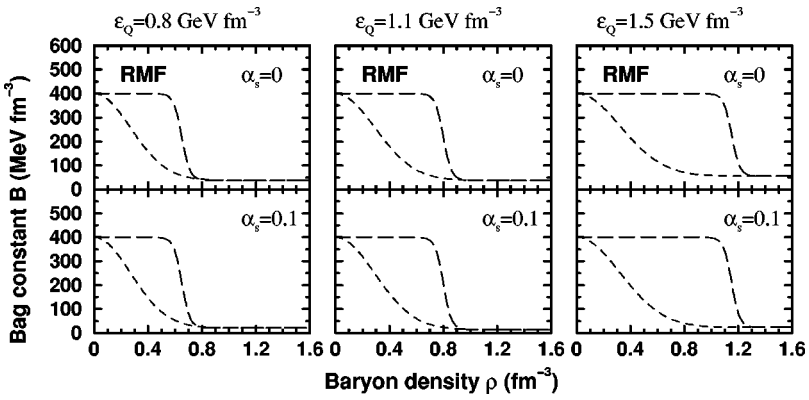

FIG. 4. Same as Fig. 3, but for the RMF nucleonic equation of state.

B_∞ can be readily calculated at the transition energy density (known from experiments), which corresponds to a value of the baryonic number density $\bar{\rho}$ given by the hadronic equation of state, i.e.,

$$B_\infty = \epsilon_Q(\bar{\rho}, x_p) - \frac{3}{4}\left[\frac{\pi^2}{(1-2\alpha_s/\pi)}\right]^{1/3} \times [(1+x_p)^{4/3} + (2-x_p)^{4/3}]\bar{\rho}^{4/3}. \quad (41)$$

Therefore we can determine a range of values for B_∞, that are shown in Table I.

We limit ourselves to consider only two possible values of α_s, i.e., $\alpha_s = 0$ and $\alpha_s = 0.1$, here and throughout this paper. Although the values of B_∞ span a wide range, we have verified that our results do not change appreciably by varying this value, since at large densities the quark matter EOS is dominated by the kinetic term on the right-hand side (RHS) of Eq. (40). With those values of B_∞ we then construct two parametrizations of B as a function of the baryon density. First, we use a Gaussian parametrization given as

$$B(\rho) = B_\infty + (B_0 - B_\infty)\exp\left[-\beta\left(\frac{\rho}{\rho_0}\right)^2\right]. \quad (42)$$

The parameter β is fixed numerically by imposing that the quark matter energy density from Eq. (40) matches the nucleonic one at the desired transition density $\bar{\rho}$. Therefore β depends only on the free parameter $B_0 = B(\rho = 0)$. However, the exact value of B_0 is not very relevant for our purpose, since at low density the matter is in any case in the nucleonic phase. In our previous paper [6] we have used both $B_0 = 200$ MeV fm^{-3} and $B_0 = 400$ MeV fm^{-3}, and found that the results did not sensitively depend on it. Therefore in this work we limit ourselves to use the value $B_0 = 400$ MeV fm^{-3}.

We also use another extreme, Woods-Saxon–like, parametrization,

$$B(\rho) = B_\infty + (B_0 - B_\infty)\left[1 + \exp\left(\frac{\rho - \tilde{\rho}}{\rho_d}\right)\right]^{-1}, \quad (43)$$

where B_0 and B_∞ have the same meaning as described before for Eq. (42) and $\tilde{\rho}$ has been fixed in the same way as β for the Gaussian parametrization. However, we have chosen sets of values for $\tilde{\rho}$ and ρ_d in such a way that B remains practically constant at a value B_0 up to a certain density and then drops to B_∞ almost like a step function. It is an extreme parametrization in the sense that it will delay the onset of the quark phase in neutron star matter as much as possible. The parametrizations of B [Eqs. (42) and (43)] are shown in Fig. 3 for BHF and Fig. 4 for RMF equations of state.

The complete results for the energy densities are shown in Fig. 5 for the BHF and Fig. 6 for the RMF nucleonic equation of state (solid lines). By assuming that the hadron-quark transition takes place within a range of energy density values, we have considered three possible values of the transition energy density, i.e., $\epsilon_Q = 0.8$, 1.1, and 1.5 GeV fm^{-3}. We find that at very low baryon density the quark matter energy density is higher than that of nuclear matter, while with increasing baryon density the two energy densities become equal at a certain point (indicated by the full dot), and after

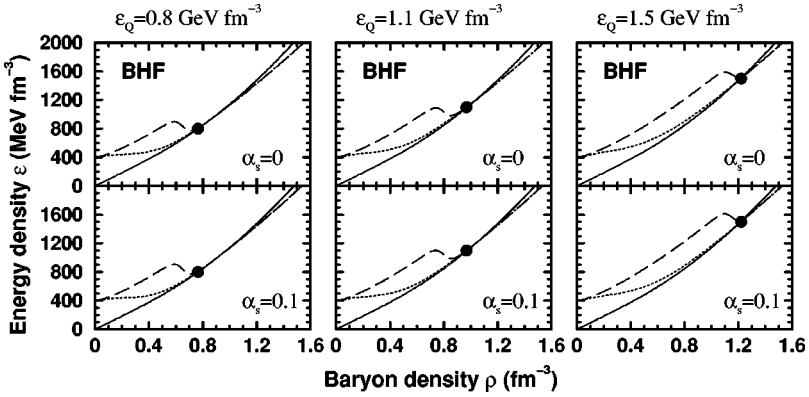

FIG. 5. The energy density is displayed vs the baryon density for almost symmetric matter ($x_p = 0.4$, solid line) in the BHF approach. The left, central, and right panels correspond to different transition energy densities $\epsilon_Q = 0.8$, 1.1, and 1.5 GeV fm^{-3}. Those values are represented by the full dots. The short (long) dashed lines represent calculations for u, d quark matter obtained within the MIT bag model, with B parametrized as a Gaussian (Woods-Saxon) function. Two values of the QCD coupling constant $\alpha_s = 0$, 0.1 are considered.

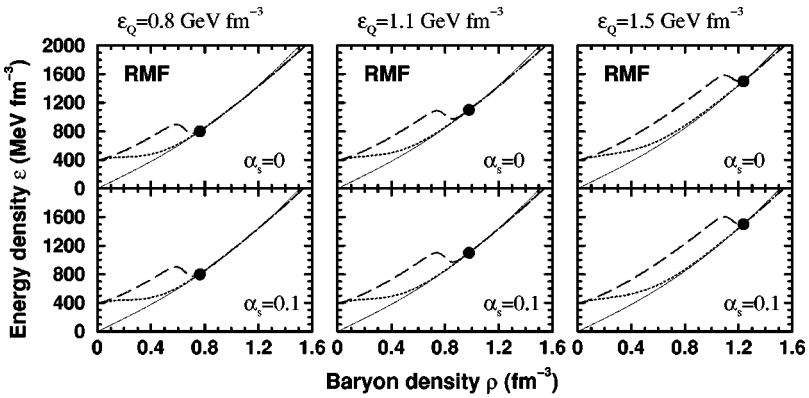

FIG. 6. Same as Fig. 5, but for the RMF hadronic equation of state with $x_p = 0.5$.

that the nuclear matter energy density remains always higher. We identify this crossing point with the transition density from nuclear matter to quark matter.

B. Phase transition in β-stable neutron star matter

With these parametrizations of the density dependence of B we now consider the hadron-quark phase transition in neutron stars. In both the BHF and the RMF approach, we calculate the EOS of a conventional neutron star as composed of a chemically equilibrated and charge neutral mixture of nucleons, hyperons, and leptons. The result is shown by the solid lines in Figs. 7 and 8, respectively.

The dotted (dashed) lines represent the EOS of β-stable and charge neutral (u,d,s) quark matter obtained within the MIT bag model, with B parametrized as a Gaussian-like (Woods-Saxon–like) function. In particular, the left-hand panels display calculations with a transition energy density $\epsilon_Q = 0.8$ GeV fm^{-3}, whereas the central panels show the results for $\epsilon_Q = 1.1$ GeV fm^{-3} and the right-hand panels for $\epsilon_Q = 1.5$ GeV fm^{-3}. Two sets of values of the s-quark mass and the QCD coupling constant α_s are considered, namely, $m_s = 150$ MeV, $\alpha_s = 0$ (upper panels) and $m_s = 200$ MeV, $\alpha_s = 0.1$ (lower panels). The full squares (diamonds) represent the crossing points between the hadron and the quark phase. They lie inside the mixed phase region, whose range, at this stage, cannot be derived from the behavior of the energy density alone. In spite of that, some qualitative considerations can be done. In fact, we notice that the mixed phase starts at values of the baryon density which increase with increasing ϵ_Q, and that those values turn out to be weakly dependent on the values of m_s and α_s. However, if $\epsilon_Q = 1.5$ GeV fm^{-3}, no phase transition at all is present when the Woods-Saxon-like parametrization of B is adopted and the BHF EOS is considered. In this case, neutron star matter always remains in the hadronic phase. This does not hold for the RMF EOS (see Fig. 8), where a well-defined phase transition is present with each parametrization chosen for B. In this case the crossing points are shifted to values of baryonic densities slightly smaller than in the BHF case. Therefore, in the RMF case, the onset of the mixed phase should start earlier.

Now we are ready to perform the Glendenning construction [34], which determines the range of baryon density where both phases coexist. The essential point of this procedure is that both the hadron and the quark phase are allowed to be separately charged, still preserving the total charge neutrality. This implies that neutron star matter can be treated as a two-component system, and therefore can be parametrized by two chemical potentials. Usually one chooses the pair (μ_e, μ_n), i.e., electron and baryon chemical potentials. The

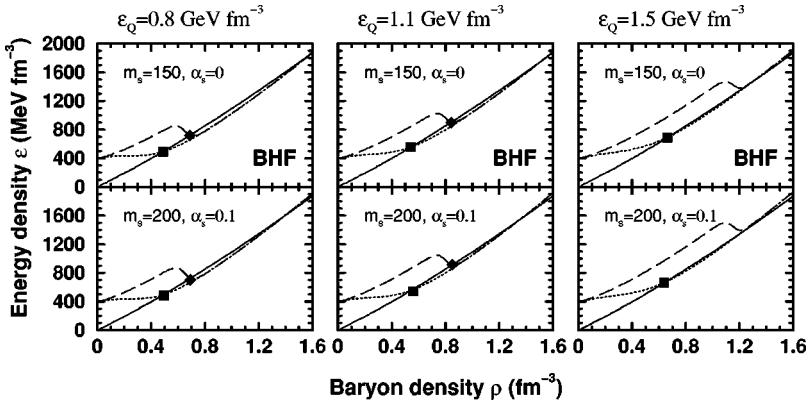

FIG. 7. The energy density is displayed vs the baryon density for β-stable matter in the BHF approach (solid line). The dotted (dashed) lines represent calculations for u, d, s quark matter obtained within the MIT bag model, with B parametrized as a Gaussian-like (Woods-Saxon–like) function. The left, central, and right panels correspond to different transition energy densities $\epsilon_Q = 0.8$, 1.1, and 1.5 GeV fm^{-3}. The full squares (diamonds) are the crossings between the hadron and the quark phase. Two sets of values of the s-quark mass and QCD coupling constant are considered; $m_s = 150$ MeV, $\alpha_s = 0$ (upper panels) and $m_s = 200$ MeV, $\alpha_s = 0.1$ (lower panels). See text for details.

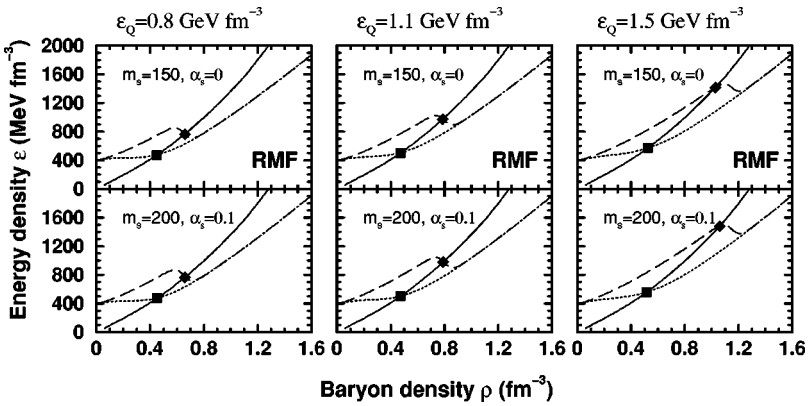

FIG. 8. Same as Fig. 7, but for the RMF baryonic equation of state.

pressure is the same in the two phases to ensure mechanical stability, while the chemical potentials of the different species are related to each other satisfying chemical and β stability. The Gibbs condition for mechanical and chemical equilibrium at zero temperature between both phases reads

$$P_{\mathrm{HP}}(\mu_e,\mu_n)=P_{\mathrm{QP}}(\mu_e,\mu_n)=P_{\mathrm{MP}}. \tag{44}$$

From this equation we can calculate the equilibrium chemical potentials of the mixed phase corresponding to the intersection of the two surfaces representing the hadron and the quark phase. At densities below the mixed phase, the system is in the charge neutral hadronic phase, and above the pressure of the charge neutral quark phase is higher than the one in the mixed phase. Therefore the system is in the quark phase. The intersection of the two surfaces allows one to calculate the charge densities ρ_c^{HP} and ρ_c^{QP} and therefore the volume fraction χ occupied by quark matter in the mixed phase, i.e.,

$$\chi\rho_c^{\mathrm{QP}}+(1-\chi)\rho_c^{\mathrm{HP}}=0. \tag{45}$$

From this, the energy density ϵ_{MP} and the baryon density ρ_{MP} of the mixed phase can be calculated as

$$\epsilon_{\mathrm{MP}}=\chi\epsilon_{\mathrm{QP}}+(1-\chi)\epsilon_{\mathrm{HP}}, \tag{46}$$

$$\rho_{\mathrm{MP}}=\chi\rho_{\mathrm{QP}}+(1-\chi)\rho_{\mathrm{HP}}. \tag{47}$$

The resulting EOS's for neutron star matter, according to the different bag parametrizations and hadronic EOS's, are reported in Figs. 9, 10, and 11 for $\epsilon_Q=0.8$, 1.1, and 1.5 GeV fm^{-3}, respectively. In those figures, we display the pressure versus the baryon density for the chosen parametrizations of *B*. The left(right)-hand panels represent the calculations performed with the BHF (RMF) EOS. The shaded area represents the mixed phase. A pure quark phase is present at densities above the shaded area and a pure hadronic phase is present below it.

We note that, for a low transition density $\epsilon_Q=0.8$ GeV fm^{-3} (see Fig. 9), the pure hadron phase can be completely absent in some cases (see panels a,b,c,e), whereas in the other cases (panels d,f,g,h) a small hadronic component is always present. The mixed phase starts at low baryon densities, well below the threshold for hyperon formation, and extends up to 0.65 (0.77) fm^{-3} when the bag constant is parametrized with a Gaussian-like (Woods-Saxon–like) function. This result holds for both the BHF and RMF description of the hadronic phase. Therefore, when the quark-hadron transition takes place at $\epsilon_Q=0.8$ GeV fm^{-3} in symmetric matter, the corresponding neutron stars are characterized in some cases by the absence of a crust, with a mantle made of a mixed phase plus a pure quark phase in the core. In other cases, neutrons stars will have a crust and a very thin, purely hadronic layer, followed by a large mixed phase and a heavy quark core.

When the transition in symmetric matter takes place at

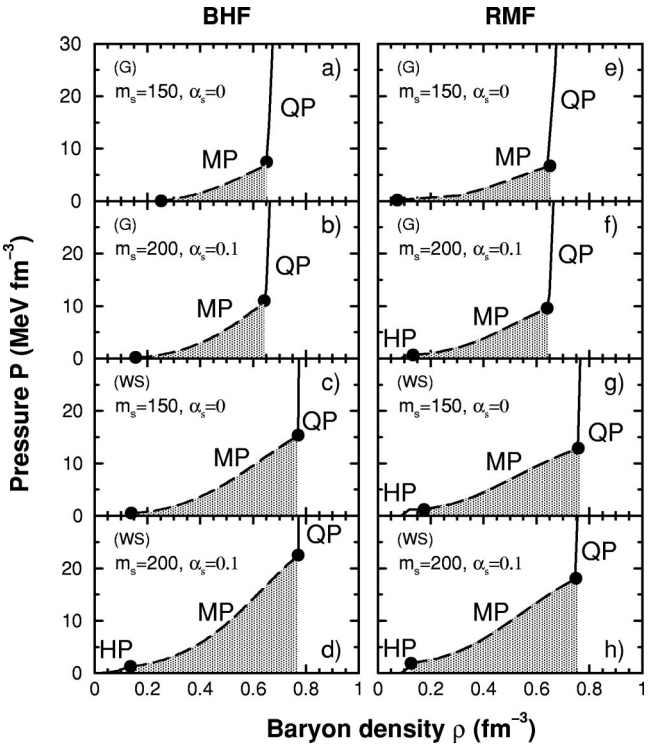

FIG. 9. The total EOS including both hadronic and quark components is displayed for a transition energy density $\epsilon_Q=0.8$ GeV fm^{-3}. Different prescriptions for the quark phase are considered, whereas the hadronic phase is described within the BHF (left-hand panels) and the RMF (right-hand panels) approaches. In all cases the shaded region, bordered by two dots, indicates the mixed phase MP, while HP and QP label the portions of the EOS where pure hadron or pure quark phases are present.

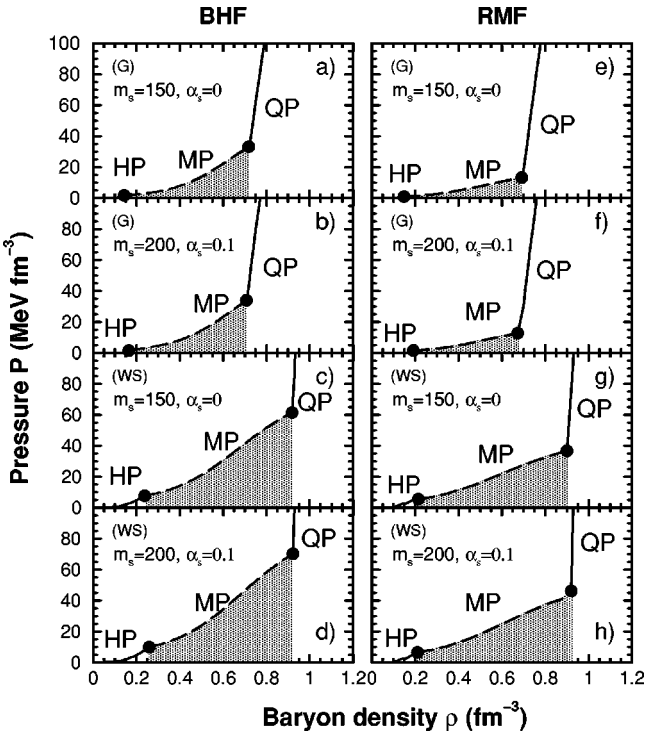

FIG. 10. Same as Fig. 9, but for $\epsilon_Q = 1.1$ GeV fm^{-3}.

$\epsilon_Q = 1.1$ GeV fm^{-3} (Fig. 10) [6], we observe naturally a shift of the onset of the mixed phase towards larger baryonic densities, although it turns out to be still slightly smaller than the density for hyperon formation in pure hadronic matter. Of course hyperons are still present in the hadron component of the mixed phase. In particular, when the Gaussian-like (Woods-Saxon-like) parametrization of the bag constant B is used, the mixed phase extends from 0.15–0.2 (0.21–0.25) fm^{-3} up to 0.7 (0.9) fm^{-3}, with a slight dependence on the s-quark mass and the QCD coupling constant α_s. In all cases, from Fig. 10 we notice that the hadronic phase is always present, although it is limited to a narrow range of low densities. In this case, neutron stars will always possess a hadronic layer and a crust.

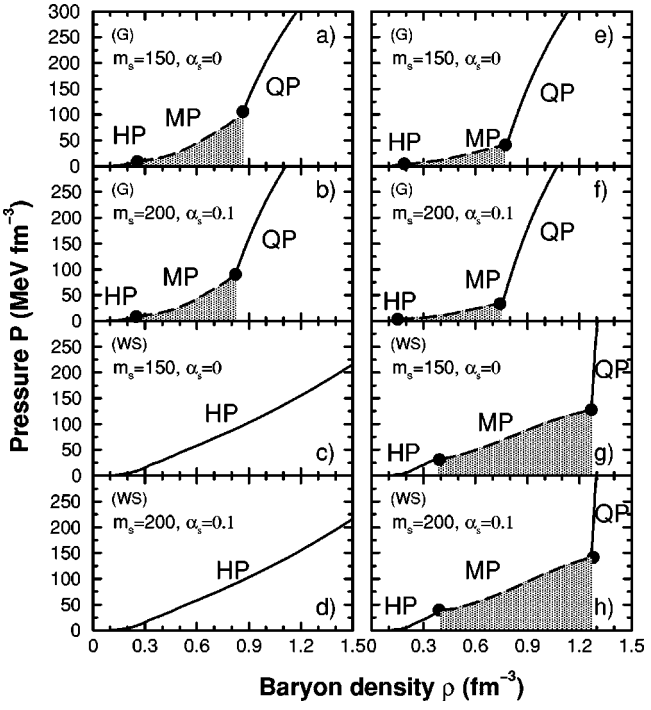

FIG. 11. Same as Fig. 9, but for $\epsilon_Q = 1.5$ GeV fm^{-3}.

Finally, when the transition in symmetric matter takes place at $\epsilon_Q = 1.5$ GeV fm^{-3} (Fig. 11), a new scenario can appear. In fact, when the Woods-Saxon–like parametrization is used for B and the BHF EOS is used for the hadronic component (panels c, d), no phase transition to quark matter is observed, and neutron star matter remains in the hadronic phase. Pure hyperon stars are then produced. In the RMF case (panels g, h) the onset of the mixed phase is shifted to 0.4–0.47 fm^{-3} and extends up to about 1.25 fm^{-3}. This gives rise to neutron stars with a thick hadronic layer. However, when the Gaussian-like parametrization is used, the mixed phase starts at the same low densities as before and extends up to 0.84 (0.77) fm^{-3} when the BHF (RMF) EOS is adopted.

Therefore, when the Gaussian-like parametrization of B is used, the onset of the mixed phase is localized at low densities and remains almost constant with changing the transition energy density in symmetric matter. If a Woods-Saxon–like parametrization is chosen, the mixed phase will start at higher baryon densities, its value changing according to the value of the transition energy density in symmetric matter. In this way, we are exploring a whole set of possible scenarios of quark-hadron phase transitions, and a corresponding set of neutron star configurations.

It has to be stressed that when the Gaussian parametrization for B is used, the density of the hadron component reaches only moderate high values. The highest value is obtained at the end of the mixed phase, where pure quark matter appears. When the transition density is fixed at $\epsilon_Q = 1.1$ GeV fm^{-3}, this maximum hadron density is about 2.5 times the saturation density, with no hyperon component. For such a range of density the hadron EOS can be considered well established, with only little uncertainities. When $\epsilon_Q = 1.5$ GeV fm^{-3} is assumed, the maximum hadron density is about 4 times saturation density, but with a 20% content of hyperons. For these density values the microscopic theories can still produce reliable predictions on the hadron EOS. Similar considerations apply when the Wood-Saxon parametrization is considered, except of course when no mixed phase is present. This parametrization, however, has to be considered less realistic, since it is devised to shift to artificially high density the onset of the quark phase.

C. Structure of neutron stars

We assume that a neutron star is a spherically symmetric distribution of mass in hydrostatic equilibrium. The equilibrium configurations are obtained by solving the Tolman-Oppenheimer-Volkoff (TOV) equations [1] for the pressure P and the enclosed mass m,

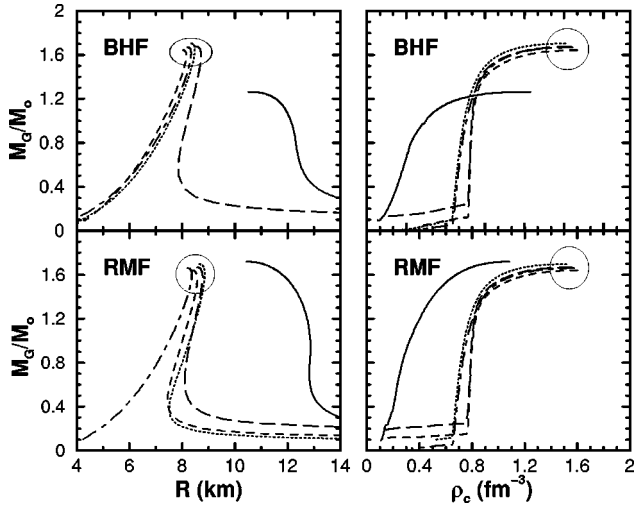

FIG. 12. The mass-radius (left panels) and mass-central density (right panels) relations are displayed for $\epsilon_Q = 0.8$ GeV fm^{-3} and several parametrizations of the bag constant B. In particular the dot-dashed (dotted) lines represent the calculations performed with $m_s = 150$ MeV, $\alpha_s = 0$ ($m_s = 200$ MeV, $\alpha_s = 0.1$) and the Gaussian-like parametrization of B, whereas the dashed (long-dashed) lines represent the calculations performed with $m_s = 150$ MeV, $\alpha_s = 0$ ($m_s = 200$ MeV, $\alpha_s = 0.1$) and the Woods-Saxon–like parametrization of B. Calculations performed with the BHF (RMF) EOS for the hadronic component are displayed in the upper (lower) panels by the solid lines.

$$\frac{dP(r)}{dr} = -\frac{Gm(r)\epsilon(r)}{r^2} \times \frac{[1+P(r)/\epsilon(r)][1+4\pi r^3 P(r)/m(r)]}{1-2Gm(r)/r}, \tag{48}$$

$$\frac{dm(r)}{dr} = 4\pi r^2 \epsilon(r), \tag{49}$$

G being the gravitational constant. Starting with a central mass density $\epsilon(r=0) \equiv \epsilon_c$, we integrate out until the pressure on the surface equals that corresponding to the density of iron. This gives the stellar radius R and the gravitational mass is then

$$M_G \equiv m(R) = 4\pi \int_0^R dr\, r^2 \epsilon(r). \tag{50}$$

We have used as input the equations of state displayed in Figs. 9, 10, and 11. For the description of the NS's crust, if present, we have joined the hadronic equations of state with those by Negele and Vautherin [35] in the medium-density regime, and those by Feynman, Metropolis, and Teller [36] and Baym, Pethick, and Sutherland [37] for the outer crust.

The results are plotted in Figs. 12, 13, and 14. We display the gravitational mass M_G (in units of the solar mass $M_\odot$) as a function of the radius R (left-hand panels) and central baryon density ρ_c (right-hand panels). The solid line represents the calculation for β-stable asymmetric nuclear matter

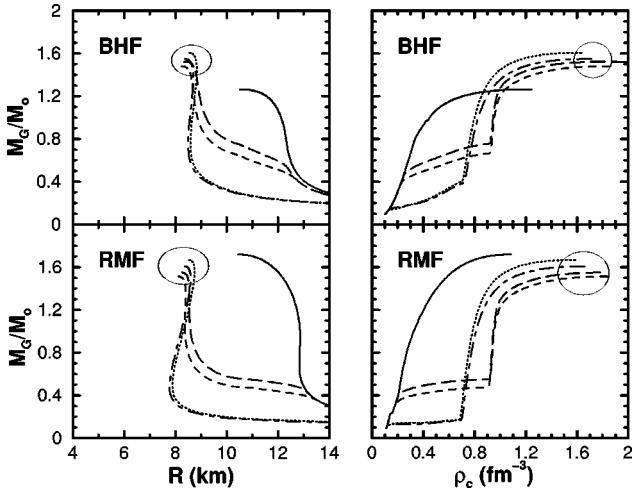

FIG. 13. Same as Fig. 12, but for $\epsilon_Q = 1.1$ GeV fm^{-3}.

including hyperons. We note that the inclusion of hyperons gives a low value of the maximum mass equal to $1.26 M_\odot$ in the BHF case. This value lies below the best observed pulsar mass, PSR1916+13, which amounts to 1.44 solar masses [38]. In the case of the RMF model, the corresponding EOS produces values of the maximum mass close to $1.7 M_\odot$.

The possible occurrence of a quark core is usually assumed to further soften the EOS and lower the maximum mass. This is indeed the case in the RMF model, as apparent in Figs. 12, 13, and 14 (lower panels). However, the situation is reversed in the BHF case, where the EOS becomes, on the contrary, stiffer. Correspondingly, the inclusion of the quark component has the effect of increasing the maximum mass in the BHF case and of decreasing it in the RMF case. This can be clearly seen in Figs. 12, 13, and 14, which display the results with a transition energy density in symmetric matter equal to 0.8, 1.1, and 1.5 GeV fm^{-3}, respectively. The maximum value of the neutron star mass lies in the range $1.44 M_\odot \leqslant M_{\max} \leqslant 1.7 M_\odot$, independent of the EOS used for the hadronic component, and no matter which parametriza-

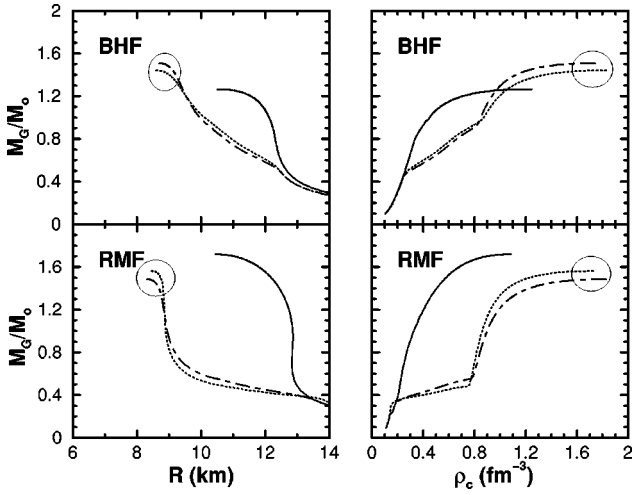

FIG. 14. Same as Fig. 12, but for $\epsilon_Q = 1.5$ GeV fm^{-3}. Only the Gaussian-like parametrizations of B are displayed.

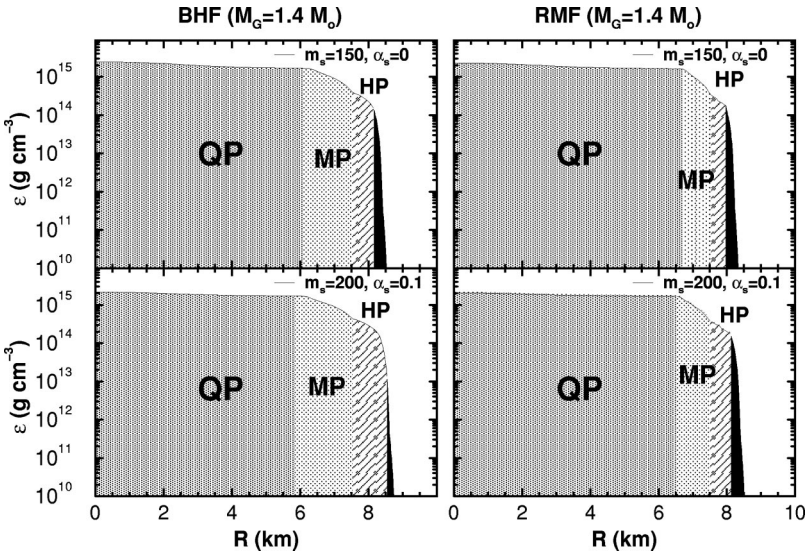

FIG. 15. Energy density profile of a neutron star with gravitational mass $M_G=1.4M_\odot$, obtained for $\epsilon_Q=1.1$ GeV fm^{-3}. In the left (right) panels the BHF (RMF) EOS has been used for describing the hadronic component, and the MIT bag model with a Woods-Saxon parametrization of B for the quark phase. Upper (lower) panels show the calculations for $m_s=150$ MeV, $\alpha_s=0$ ($m_s=200$ MeV, $\alpha_s=0.1$).

tion chosen for B. It depends only weakly on the transition energy density in symmetric matter. The configurations of the NS with a quark core are characterized by a smaller radius and a higher value of the central density, compared to the pure hadronic case (solid lines). In some cases, these stars have no crust at all, since in the EOS the hadronic component is missing.

In Fig. 15 we plot a typical density profile for a star with canonical mass $1.4M_\odot$, obtained when the transition energy density in symmetric matter is equal to 1.1 GeV fm^{-3} [6] and B has been parametrized as a Woods-Saxon–like function, with two different choices of m_s and α_s. On the left-hand panels we plot the result obtained when the BHF EOS has been used for the hadronic component, whereas on the right-hand panels the corresponding case obtained with the RMF EOS is shown. We observe that a large part of the core is composed of pure quark matter (about 6 km), then a thick layer of a couple of kilometers is in the mixed phase, followed by a modest hadronic zone and a thin crust. This generic profile turns out to be only slightly dependent on the EOS used for the hadronic component.

Some remarks should be made about the behavior of the mixed phase. As one can see clearly from Figs. 12, 13, and 14, the presence of a mixed phase produces a kind of plateau in the mass versus central density relationship, which is a direct consequence of the smaller slope displayed by all EOS's in the mixed phase region (see Figs. 9, 10, and 11). In this region, however, the pressure is still increasing monotonically, despite the apparent smooth behavior, and no unstable configuration can actually appear. We found that the appearance of this slow variation of the pressure is due to the density dependence of the bag constant, in particular the occurrence of the density derivative of the bag constant in the pressure and chemical potentials, as required by thermodynamic consistency. To illustrate this point we calculate the EOS for quark matter with a density-independent value of $B=90$ MeV fm^{-3} (see Fig. 16) and the corresponding neutron star masses. The EOS is now quite smooth and the mass versus central density shows no indication of a plateau.

Finally, it has to be pointed out that the maximum mass value, whether B is density dependent or not, is dominated by the quark EOS at densities where the bag constant is much smaller than the quark kinetic energy. The constraint coming from heavy-ion reactions, as discussed above, is relevant only to the extent that it restricts B at high density within a range of values, which are commonly used in the literature. This can be seen also from Fig. 16, where the (density independent) value of $B=90$ MeV produces again a maximum value around 1.5 solar masses.

V. CONCLUSIONS

We studied neutron star properties, in particular NS's maximum masses, using an EOS which combines reliable EOS's for hadronic matter and a bag model EOS for quark

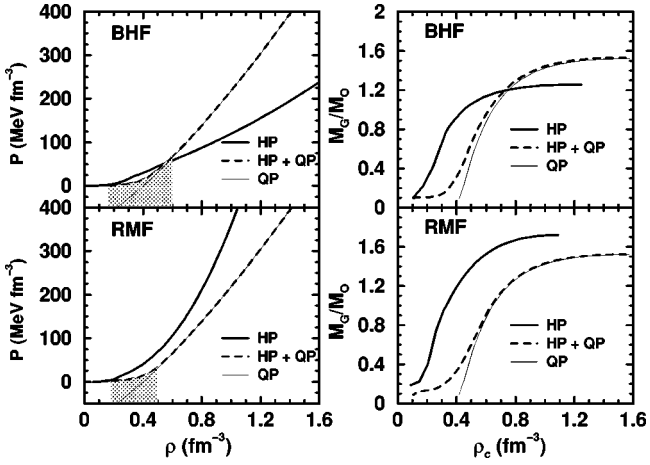

FIG. 16. In the left panel is shown the EOS for neutron star matter (dashed lines labeled by HP+QP) for a density independent value of the bag constant $B=90$ MeV fm^{-3}, with BHF and RMF hadronic equations of state. The shaded areas indicate the mixed phase region. The corresponding masses vs central densities are shown on the right panels. In all cases the thin and thick lines correspond to the results obtained for a pure quark and a pure hadron EOS, respectively.

matter. We found that a density-dependent B is necessary to get the transition to the quark-gluon plasma in nearly symmetric nuclear matter at an energy density that is well above saturation density and in a range of values that can be considered compatible with the CERN-SPS and RHIC findings on the phase transition from hadronic matter to quark matter. We considered a wide range of values, from 0.8 GeV fm^{-3} to 1.5 GeV fm^{-3}, in order to establish the sensitivity of the results on the assumed value of the transition energy density.

For a given value of the transition density for symmetric nuclear matter, the corresponding transition in neutron star matter, i.e., β-stable matter, occurs in general at substantially lower energy density. It is essential, in this respect, that in the calculations strange matter is included and allowed to develop inside neutron star matter, since the appearence of strange matter tends in general to soften the EOS. The results show that the NS maximum mass is clearly correlated with the assumed value of the transition energy density. For a given transition density, the maximum mass falls in a narrow range, nearly independent of the details of the parametrization of the bag model. As the transition density is made to vary, the value of the maximum mass is shifted. In general it decreases at increasing value of the transition energy density if the hadron EOS is computed within the microscopic BHF scheme. The trend is reversed with the hadron EOS computed within the relativistic mean field method. However, this correlation appears to be rather weak, and the full range of possible values of the maximum mass turns out to be between 1.4 and 1.7 solar masses. This is compatible with the observational data obtained so far, including the most recent ones [39].

The value of the maximum mass is mainly determined by the quark component of the neutron star and by the corresponding EOS. In this sense, one can say that the value of the neutron star maximum mass can be a good testing ground for the quark EOS, rather than the hadron EOS. Indeed, the value of the maximum mass of neutron stars obtained according to our analysis appears robust with respect to the uncertainties of the nuclear EOS, and the obtained range of values is mainly due to the uncertainties of the quark EOS. Similar conclusions have been found by other authors [40] on the basis of purely phenomenological hadronic equations of state. However, the structure and composition of the neutron stars can be quite different.

Other recent calculations of neutron star properties employing various RMF nuclear EOS's together with either effective mass bag model [41] or Nambu-Jona-Lasinio model [42] EOS's for quark matter also give maximum masses of only about $1.7M_{\odot}$, even though not constrained by hints coming from the CERN-SPS and RHIC data. Therefore, according to our results, the experimental observation of a heavy ($M > 1.8M_{\odot}$) neutron star, as claimed recently by some groups [43] ($M \approx 2.2M_{\odot}$), if confirmed, would suggest that serious drawbacks are present for the possible description of the high-density phase of quark matter within the bag model.

[1] S. L. Shapiro and S. A. Teukolsky, *Black Holes, White Dwarfs, and Neutron Stars* (Wiley, New York, 1983).

[2] E. Witten, Phys. Rev. D **30**, 272 (1984); G. Baym, E.W. Kolb, L. McLerran, T.P. Walker, and R.L. Jaffe, Phys. Lett. **160B**, 181 (1985); N.K. Glendenning, Mod. Phys. Lett. A **5**, 2197 (1990).

[3] M. Baldo, *Nuclear Methods and the Nuclear Equation of State* (World Scientific, Singapore, 1999).

[4] B.D. Serot and J.D. Walecka, Adv. Nucl. Phys. **16**, 1 (1986).

[5] A. Chodos, R.L. Jaffe, K. Johnson, C.B. Thorn, and V.F. Weisskopf, Phys. Rev. D **9**, 3471 (1974).

[6] G.F. Burgio, M. Baldo, P.K. Sahu, A.B. Santra, and H.-J. Schulze, Phys. Lett. B **526**, 19 (2002).

[7] U. Heinz and M. Jacobs, nucl-th/0002042; U. Heinz, hep-ph/0009170.

[8] See, for instance, J.P. Blaizot, nucl-th/0107025.

[9] J. Cleymans, R.V. Gavai, and E. Suhonen, Phys. Rep. **130**, 217 (1986).

[10] B. Müller, *The Physics of the Quark-Gluon Plasma*, Lecture Notes in Physics Vol. 225 (Springer, Heidelberg, 1985).

[11] D. Teaney, J. Lauret, and E.V. Shuryak, Phys. Rev. Lett. **86**, 4783 (2001); nucl-th/0110037.

[12] H.Q. Song, M. Baldo, G. Giansiracusa, and U. Lombardo, Phys. Rev. Lett. **81**, 1584 (1998); Phys. Lett. B **473**, 1 (2000); M. Baldo and G. F. Burgio, in *Physics of Neutron Star Interiors*, edited by D. Blaschke, N. Glendenning, and A. Sedrakian, Lecture Notes in Physics (Springer, Heidelberg, 2001), pp. 1–30.

[13] M. Lacombe, B. Loiseau, J.M. Richard, R. Vinh Mau, J. Côté, P. Pirès, and R. de Tourreil, Phys. Rev. C **21**, 861 (1980).

[14] J. Carlson, V.R. Pandharipande, and R.B. Wiringa, Nucl. Phys. **A401**, 59 (1983); R. Schiavilla, V.R. Pandharipande, and R.B. Wiringa, *ibid.* **A449**, 219 (1986).

[15] M. Baldo, I. Bombaci, and G.F. Burgio, Astron. Astrophys. **328**, 274 (1997).

[16] M. Baldo, G.F. Burgio, and H.-J. Schulze, Phys. Rev. C **58**, 3688 (1998); **61**, 055801 (2000).

[17] I. Vidaña, A. Polls, A. Ramos, L. Engvik, and M. Hjorth-Jensen, Phys. Rev. C **62**, 035801 (2000).

[18] P. Maessen, Th. Rijken, and J. de Swart, Phys. Rev. C **40**, 2226 (1989).

[19] J.D. Walecka, Ann. Phys. (N.Y.) **83**, 491 (1974).

[20] S.K. Ghosh, S.C. Phatak, and P.K. Sahu, Z. Phys. A **352**, 457 (1995).

[21] N.K. Glendenning, Astrophys. J. **293**, 470 (1985).

[22] N.K. Glendenning, F. Weber, and S.A. Moszkowski, Phys. Rev. C **45**, 844 (1992).

[23] J.I. Kapusta and K.A. Olive, Phys. Rev. Lett. **64**, 13 (1990); J. Ellis, J.I. Kapusta, and K.A. Olive, Nucl. Phys. **B348**, 345 (1991).

[24] D. Galetti and A.F.R. de Toledo Piza, J. Phys. G **27**, 33 (2001).

[25] P.K. Sahu, Phys. Rev. C **62**, 045801 (2000).

[26] P.K. Sahu and A. Ohnishi, Nucl. Phys. **A691**, 439 (2001).

[27] E. Fahri and R.L. Jaffe, Phys. Rev. D **30**, 2379 (1984).

[28] H. Satz, Phys. Rep. **89**, 349 (1982).

[29] G.X. Peng, H.C. Chiang, B.S. Zou, P.Z. Ning, and S.J. Luo, Phys. Rev. C **62**, 025801 (2000).
[30] J. Rafelsky and B. Müller, Phys. Rev. Lett. **48**, 1066 (1982); T. Matsui and H. Satz, Phys. Lett. B **178**, 416 (1986).
[31] M. Alford, Annu. Rev. Nucl. Part. Sci. **51**, 131 (2001); K. Rajagopal and F. Wilczek, in *At the Frontier of Particle Physics: Handbook of QCD*, edited by M. Shifman (World Scientific, Singapore, 2001).
[32] C. Adami and G.E. Brown, Phys. Rep. **234**, 1 (1993); Xue-min Jin and B.K. Jennings, Phys. Rev. C **55**, 1567 (1997).
[33] D. Blaschke, H. Grigorian, G. Poghosyan, C.D. Roberts, and S. Schmidt, Phys. Lett. B **450**, 207 (1999).
[34] N.K. Glendenning, Phys. Rev. D **46**, 1274 (1992).
[35] J.W. Negele and D. Vautherin, Nucl. Phys. **A207**, 298 (1973).
[36] R. Feynman, F. Metropolis, and E. Teller, Phys. Rev. **75**, 1561 (1949).
[37] G. Baym, C. Pethick, and D. Sutherland, Astrophys. J. **170**, 299 (1971).
[38] R.A. Hulse and J.H. Taylor, Astrophys. J. Lett. **195**, L51 (1975).
[39] J.A. Orosz and E. Kuulkers, Mon. Not. R. Astron. Soc. **305**, 132 (1999); O. Barziv, L. Kaper, M.H. van Kerkwijk, J.H. Telting, and J. van Paradijs, Astron. Astrophys. **377**, 925 (2001).
[40] A. Rosenhauer, E.F. Staubo, and L.P. Csernai, Z. Phys. A **342**, 235 (1992).
[41] K. Schertler, C. Greiner, P.K. Sahu, and M.H. Thoma, Nucl. Phys. **A637**, 451 (1998); K. Schertler, C. Greiner, J. Schaffner-Bielich, and M.H. Thoma, *ibid.* **A677**, 463 (2000).
[42] K. Schertler, S. Leupold, and J. Schaffner-Bielich, Phys. Rev. C **60**, 025801 (1999).
[43] P. Kaaret, E. Ford, and K. Chen, Astrophys. J. Lett. **480**, L27 (1997); W. Zhang, A.P. Smale, T.E. Strohmayer, and J.H. Swank, *ibid.* **500**, L171 (1998).